Journal of
Applied Research in Water and Wastewater
Journal homepage: www.arww.razi.ac.ir

Physical and numerical modeling for the investigation of downstream scour caused by sudden blockage in circular and box culvert inlets

Saeed Gohari*, Somayeh Karimpour

Department of Water Engineering, College of Agriculture, Bu-Ali Sina University, Hamadan, Iran.

GRAPHICAL ABSTRACT

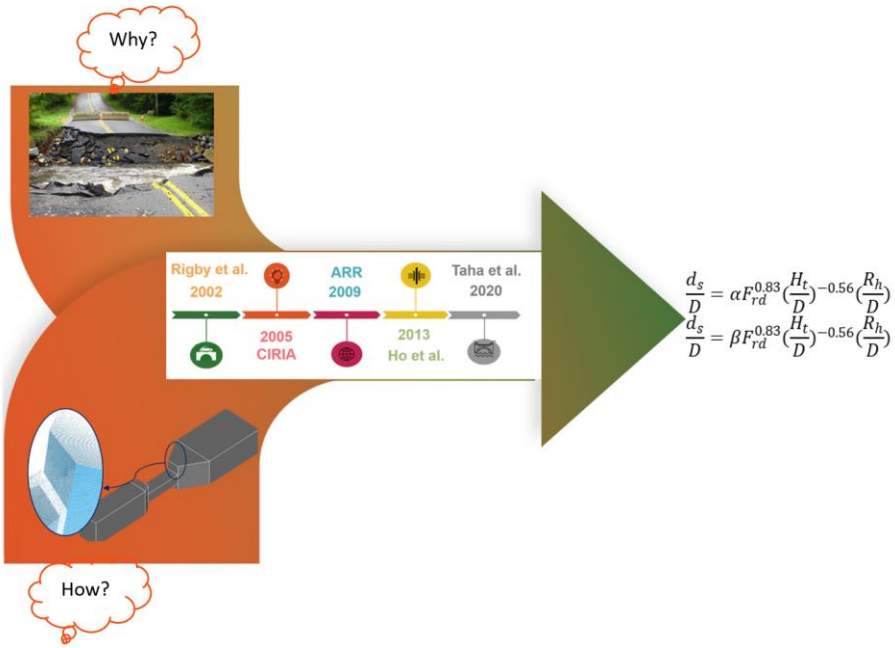

ARTICLE INFO

Article type:
Research Article

Article history:
Received 17 March 2025
Received in revised form 20 May 2025
Accepted 21 May 2025
Available online 1 June 2025

Keywords:
Barrel shape
Culvert
VOF
Scour
RANS

ABSTRACT

This paper presents a comprehensive experimental and numerical study using non-cohesive uniform sand (d50 = 2 mm). The study investigates the impact of local scour downstream of four model culverts with different barrel shapes and inlet blockage sizes. The results show that, for clear water scour, the shape and number of culvert barrels affect downstream scour geometry. The most affected parameters of scour hole geometry in blocked inlet culverts were the maximum scour depth near the walls (d_{swall}) and the maximum scoured sediment volume (ζs). The d_{swall}/D values of rectangular model culverts were 1.3 to 1.5 times greater than those of circular model culverts. The results showed that the effect of inlet obstruction on d_{smax} is contingent on flow and culvert conditions. Based on this, a suitable relationship was proposed to estimate the maximum scour depth for each cross-section. The presented equations were compared to the existing equation based on inlet blockage by applying collected datasets and they showed superior performance. The comparison indicated that over 80% of the predicted values fall within ±30% error lines.

1. Introduction

Scouring in the vicinity of hydraulic structures, abutments, and piers is still one of the most important issues that affect the stability of structures. There are valuable investigations on scour processes downstream of culverts (Bodhaine, 1968; Hotchkiss and Larson and Admiral, 2005; Pagliara and Carnacina, 2011; Barthelmess and Rigby, 2011; Wang and Uys and Chanson, 2018; Wallerstein and Arthur, 2018). Scouring is a process directly related to the power of the flow. This principle has been introduced from the first studies done in this field (Smith, 1957) to the present studies, such as Hotchkiss and Larson and Admiral, 2005, who worked on energy dissipation in culverts by creating a forced hydraulic jump inside the barrel. This will lead to a decrease in the risk of scouring downstream of the culvert. Other studies have shown the effect of turbulence intensity on increasing the size of the scour hole. In this regard, Liriano and Day and White, 2002 studied scour at culverts influenced by turbulent flow and pointed out that the peak values of turbulence intensities over the fixed bed coincide

*Corresponding author Email: s.gohari@basu.ac.ir

Cite this article: S. Gohari, S. Karimpour, Physical and numerical modeling for the investigation of downstream scour caused by sudden blockage in circular and box culvert inlets, *Journal of Applied Research in Water and Wastewater*, 12 (1), 2025, 114-127. doi: https://doi.org/10.22126/arww.2025.12040.1367

with the location of the maximum scour depth for the fully developed scour hole. Obstruction at the culvert inlet increases the effect of both factors by increasing the amount of energy difference. There are valuable investigations on debris and blockage issues that seek to explain how structures in urban watercourses and rural rivers become blocked with different types of debris (Allen *et al.,* 2015; Armitage and Rooseboom, 1999; CIRIA, 2010). Based on the maintenance and flood management manuals presented by authorities such as Australian Rainfall and Runoff (ARR, 2009), the Environment Agency (CIRIA, 2010), and the Construction Industry Research and Information Association (CIRIA 2010), blockage in watercourses is one of the most significant parameters in flood management. Additionally, there is a valuable literature review on culvert blockage using laboratory and field data from cases such as Ho and Muste and Ettema, 2013; Streftaris *et al*., 2012; Rigby, and Barthelmess, 2011, which investigate the catchment characteristics that affect blockage in culverts and watercourses. Nevertheless, there is not a wide literature review on the side effects of blockages in drainage system structures, especially in culverts. Culverts are highly prone to sudden blockage by various sources of debris and drift. Sorourian and Keshavarzi and Ball, 2015 investigated the effect of sudden debris accumulation at a culvert inlet on downstream scour. They reported that the dimensions of the scour hole changed under the partially blocked inlet and evaluated an equation for the maximum depth of the scour hole based on the densimetric Froude number and blockage. They referred to higher turbulent energy values to explain the larger dimensions of the scour hole in the blocked inlet culvert. Galan and Gonzalez examined the effects of blockage, culvert shape, and wing walls on outlet scouring in non-submerged outlet conditions. Their study focused on embankment undermining and analyzed 80 test results using ANOVA techniques. The importance of wing walls with a flat slab and inlet blockage was highlighted. The influence of tailwater depth and culvert shape on the scour hole was confirmed as relevant factors, as well as the presence of wing walls. The main outcome of their work was the identification of factors and interactions that have a significant impact on local scour at the culvert outlet. Taha et al., 2020 conducted a thorough study to investigate the effect of inlet obstruction on downstream scouring in rectangular and circular culverts. Their most important conclusion was that the maximum scour depth increases less than expected compared to other parameters.

Based on previous studies in the field, the current study addresses the downstream scour of culverts under the effect of inlet blockage in both rectangular and circular culverts using experimental and numerical models.

2. Material and methods

2.1. Experimental setup

All tests were conducted in the Hydraulic Laboratory of the Water Engineering Department at Bu Ali Sina University, Hamedan, Iran. The box culvert models were made of glass, while smooth water pipes were used as circular culvert models. The experimental setup included a glass-wall flume with a length of 10 m, a width of 0.5 m, and a height of 0.6 m. An inverter motor pump system supplied the flume with a maximum discharge of 60 l/s. The magnitude of the discharge was controlled directly by the inverter system. Additionally, there was a calibrated triangular weir downstream of the flume for discharge measurement. The water level in the flume was controlled by a sluice gate located downstream of the flume. The movable bed at the culvert outlet consisted of uniform sand with d50 = 2 mm and σg = 1.2, with dimensions of 2.5 m in length, 0.5 m in width, and 0.15 m in height. To prevent sediment from entering the tank, a sediment trapper was used at the end of the movable bed. According to the results of Day and Liriano and White, 2001's study on the effects of scale and tailwater depth on culvert outlet scouring, the downstream water level was considered to be exceed 70 mm. Their results indicated that in tailwater values of less than 15 mm and a Reynolds number in the barrel of fewer than 104, the experiments were affected by model scale [6]. The ratio of the width of the culvert to the width of the canal for flow modeling in the culvert ranges from 0.3 - 0.5 to a maximum of 2 - 2.9; whereas in the current study, it was 0.3 (CIRIA, 2010) The culvert cross-section was designed according to the design considerations provided by Bodhaine, 1968, based on the flow regime in the culvert and the available laboratory facilities. Since the purpose was to study the obstruction at the inlet of the culvert, the models were designed for inlet control. Flow conditions were determined using Bodhaine, 1968's first type of flow as defined in Eq. 1 and Fig. 1.

$$Q = CA\sqrt{2g(h_1 - z - d_c - h_{f1,2} + \alpha\frac{V_1^2}{2g})} \quad (1)$$

where, Q, C, A, h_1, z, d_c, $h_{f1,2}$, α and V_1 are discharge, conveyance coefficient, cross- sectional area, upstream water elevation, culvert bottom elevation, critical depth at the culvert inlet, energy loss between points 1 and 2 (Fig. 1), kinetic energy correction coefficient and velocity in culvert inlet, respectively.

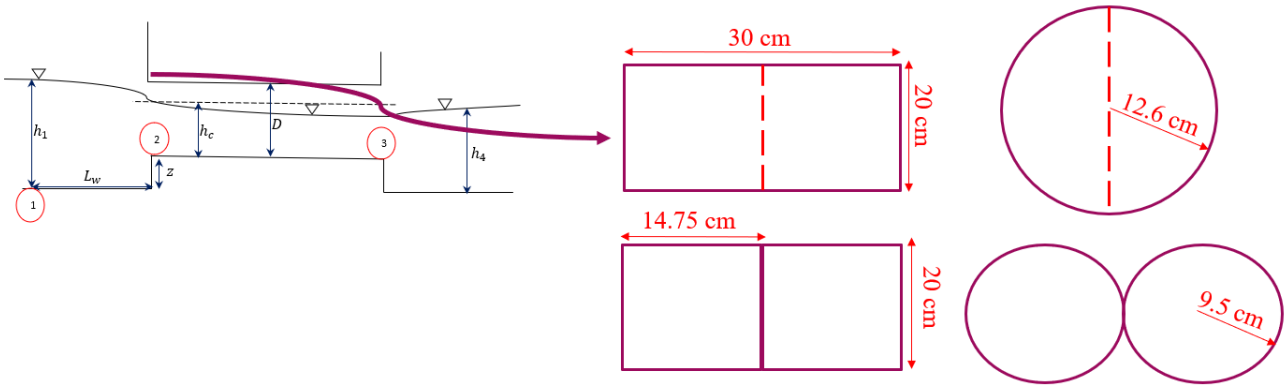

Fig. 1. Flow condition and designed cross sections.

The cross-sectional area of the models was determined based on the maximum discharge. Table 1 shows the geometric characteristics of all model culverts used in this study.

Table1. Cross section characteristics.

Model culvert	Total area, cm^2	Total perimeter, cm	Hydraulic radius, cm
One Barrel Box(R1)	600	100	8.6
Two Barrel Box(R2)	580	138	4.2
One Barrel Circular(C1)	573	84.8	6.8
Two Barrel Circular(C2)	566	119.3	4.7

Four different blockage scenarios were used for the blockage simulation which, covering 20%, 40%, 60% and 80% of the inlet area. Three discharge values, including Q_d(design discharge for each cross-section), $0.6Q_d$ and $0.4Q_d$ were applied for the experimental setup. The experimental properties are presented in the Table 2.

Uniform, non-cohesive sand was used as the bed material, with a particle size of 2 mm. Based on the initial 72-hour tests and previous research (Melville and Lim, 2013 and Liriano and Day and White, 2002), the test time was considered to be 6 hours, with a scour depth of 95% of the maximum scour depth.

2.2. Dimensional analysis

Variation of scour hole geometry can be analyzed by major scour factors such as the scour area, the scour longitudinal profile, the volume of transported sediment, and the maximum depth of scour. Effective

parameters include barrel geometry, outlet type and flow geometry, and bed material characteristics.

Table 2. Properties of experimental tests.

Test	F_{rd}	H_u, cm	H_d, cm	u^*/u^*_c
R1Q10.5B0	2.78	25.40	7.90	0.72
R1Q10.5B20	4.52	28.50	7.90	0.51
R1Q10.5B40	5.26	31.60	8.80	0.53
R1Q10.5B80	4.86	40.50	9.00	0.54
R1Q16.5B0	2.96	28.40	11.00	0.63
R1Q16.5B20	4.71	31.40	9.80	0.62
R1Q16.5B40	5.39	34.30	9.00	0.62
R1Q16.5B60	5.93	38.50	11.50	0.61
R1Q27.5B0	3.38	34.80	15.50	0.72
R1Q27.5B20	3.38	36.50	15.50	0.72
R1Q27.5B40	3.17	38.80	16.90	0.75
R1Q27.5B60p	3.17	39.40	17.20	0.75
R2Q10.5B0	2.78	25.50	8.00	0.50
R2Q10.5B20	4.32	28.50	7.60	0.50
R2Q10.5B80	4.63	39.30	8.00	0.50
R2Q16.5B0	2.88	28.60	10.30	0.60
R2Q16.5B20	4.23	31.40	11.00	0.60
R2Q16.5B60	5.93	38.00	11.50	0.60
R2Q27.5B0	3.13	34.80	17.00	0.75
R2Q27.5B20	3.17	36.50	17.00	0.74
R2Q27.5B60p	3.17	40.50	17.00	0.74
C1Q10.5B0	3.11	29.20	8.00	0.69
C1Q16.5B0	3.48	32.50	12.50	0.77
C1Q27.5B0	4.63	35.50	14.90	0.73
C1Q10.5B20	3.04	30.80	8.00	0.72
C1Q16.5B20	4.46	34.20	11.50	0.69
C1Q27.5B20	5.47	37.20	14.00	0.69
C1Q10.5B60	3.04	36.70	9.70	0.71
C1Q16.5B60	3.86	40.00	12.50	0.78
C1Q27.5B60p	5.47	39.10	15.20	0.71
C2Q10.5B0	1.41	26.40	8.80	0.76
C2Q16.5B0	1.62	29.20	11.40	0.81
C2Q27.5B0	2.09	32.80	14.00	0.75
C2Q10.5B20	1.24	28.50	9.40	0.80
C2Q16.5B20	1.70	31.00	11.50	0.79
C2Q27.5B20	1.87	34.00	14.90	0.78
C2Q10.5B60	1.41	34.00	9.50	0.76
C2Q16.5B60	1.68	38.00	11.50	0.83
C2Q27.5B60p	1.87	37.00	15.20	0.78

Therefore, a set of effective parameters for downstream scouring phenomena can be proposed as follows:

$$\{Q, H_u, H_t, W, D, S, L, \rho, g, \theta, d_{50}, \rho_s, L_s, \omega_s, \zeta_s, \chi_s, d_s, d_{swall}\} \quad (2)$$

In the presence of debris accumulation at the culvert inlet, the blockage factor must also be added to these parameters. The geometric parameter in the culvert barrel that is most affected by the presence of blockage is the hydraulic radius at the outlet; thus, (R_h/D) is another effective dimensionless parameter. According to Smith's study on scouring progress in the culvert downstream jet, the most effective parameters are the energy of the water jet and the downstream submergence condition related to tailwater depth (Barthelmess and Rigby, 2011). Based on this brief arrangement, the energy equation between the culvert inlet and outlet is defined as:

$$H_{up} + \frac{V_{up}^2}{2g} - h_l = H_{down} + \frac{V_{down}^2}{2g} \quad (3)$$

where, H is the water surface elevation, V is the mean velocity, and the up and down subscripts refer to the upstream and downstream of the culvert; g is the acceleration due to gravity, and h_l is the head loss, which includes section friction loss, inlet and outlet head loss, and the energy loss of the hydraulic jump. The dimensionless energy parameter is defined as:

$$\frac{\Delta E}{E_o} = \frac{E_{upstream,B} - E_{downstream,B}}{E_o} \quad (4)$$

$E_{upstream,B}$ is the total hydraulic energy at the upstream with debris accumulation (B), $E_{downstream,B}$ is the total hydraulic energy at the downstream in the presence of debris accumulation (B) and E_o is the difference between the upstream and downstream energy values under the same flow conditions without any debris. Instead of H_u, the relative total energy of flow $\Delta E/E_o$ is used in the dimensional analysis of this phenomena. Finally, the dimensionless parameters for the scour hole geometry are as follows:

$$\psi(d_s/D, d_{swall}/D, L_s/D, \omega_s/D, \chi_s/D, A_s/D^2, \zeta_s/D^3, Fr_d, R_h/D, \Delta E/E_o, h_t/D, d_{50}/D) = 0 \quad (6)$$

All tests were conducted under clear water conditions ($0.6 < U/U_c < 1$) to observe the effects of barrel shape and inlet blockage on downstream scouring in different flow conditions. According to Melville and Lim, 2013's research, the maximum scour hole depth is independent of sediment size when d50/D < 0.6, which in the current study is equal to 0.1.

2.3. Numerical implementation

The OpenFOAM hydrodynamic model is used to simulate flow and sediment transport. Fluid motion is mathematically described by the continuity and momentum equations from the Eulerian approach. In incompressible flow, the fluid density becomes an independent variable. Newton's second law states that the rate of momentum is proportional to the fluid forces. The Eq.7- 11represent 3D equations of motion, including volume and area fractions as below:

$$\frac{\partial(uA_x)}{\partial x} + \frac{\partial(vA_y)}{\partial y + \frac{\partial(wA_z)}{\partial z}} = 0 \quad (7)$$

$$\frac{\partial u}{\partial t} + \left(\frac{uA_x}{\forall_f}\left(\frac{\partial u}{\partial x}\right) + \frac{vA_y}{\forall_f}\left(\frac{\partial u}{\partial y}\right) + \frac{wA_z}{\forall_f}\left(\frac{\partial u}{\partial z}\right)\right) = -\frac{\forall_f}{\rho}\left(\frac{\partial p}{\partial x}\right) + \frac{\mu}{\rho}\left(\frac{\partial^2(A_x u)}{\partial x^2} + \frac{\partial^2(A_y u)}{\partial y^2} + \frac{\partial^2(A_z u)}{\partial z^2}\right) + g_x \quad (8)$$

$$\frac{\partial v}{\partial t} + \left(\frac{uA_x}{\forall_f}\left(\frac{\partial v}{\partial x}\right) + \frac{vA_y}{\forall_f}\left(\frac{\partial v}{\partial y}\right) + \frac{wA_z}{\forall_f}\left(\frac{\partial v}{\partial z}\right)\right) = -\frac{\forall_f}{\rho}\left(\frac{\partial p}{\partial y}\right) + \frac{\mu}{\rho}\left(\frac{\partial^2(A_x v)}{\partial x^2} + \frac{\partial^2(A_y v)}{\partial y^2} + \frac{\partial^2(A_z v)}{\partial z^2}\right) + g_y \quad (9)$$

$$\frac{\partial w}{\partial t} + \left(\frac{uA_x}{\forall_f}\left(\frac{\partial w}{\partial x}\right) + \frac{vA_y}{\forall_f}\left(\frac{\partial w}{\partial y}\right) + \frac{wA_z}{\forall_f}\left(\frac{\partial w}{\partial z}\right)\right) = -\frac{\forall_f}{\rho}\left(\frac{\partial p}{\partial z}\right) + \frac{\mu}{\rho}\left(\frac{\partial^2(A_x w)}{\partial x^2} + \frac{\partial^2(A_y w)}{\partial y^2} + \frac{\partial^2(A_z w)}{\partial z^2}\right) + g_z \quad (10)$$

$$\forall_f \frac{\partial F}{\partial t} + \nabla.(AUF) = 0 \quad (11)$$

where, V_f *and* A_x, A_y *and* A_z, are volume and area fractions *in* the *x, y* and *z* directions $u, v, w, p, \upsilon, \rho$, g_x, g_y and g_z represent the velocity components, pressure, kinematic viscosity, fluid density and body accelerations, respectively. In turbulent flow, the kinematic viscosity is equal to $\upsilon = \frac{S_c \mu}{\rho}$, where $\frac{\upsilon_t}{K_{ed}}$ denotes the Schmidt's number S_c. In this relation, υ_t and K_{ed} represent the eddy viscosity and diffusivity, respectively (Liriano and Day and White, 2002). The VOF method is based on the donor-acceptor cells regarded as an advection scheme. In this context, the scalar function *F* represents the cells containing the fluid, while the marking of acceptor and donor cells is based on the flow passing through them. Accordingly, the acceptors receive the fluid while the donors lose it. The advection equation (Eq. 11) should be tackled to calculate F by assuming that the flow is incompressible.

2.2.1. Turbulence modeling

The Reynolds stresses are proportional to the product of the eddy viscosity $\upsilon_t = 0.09\frac{k_t^2}{\varepsilon_t}$ in the mean rate of deformations, where $k_t$andε_t represent the turbulence energy and dissipation, respectively.

$$\frac{\partial k_t}{\partial t} + \left(\frac{1}{\forall_f}\right)\left(uA_x\frac{\partial k_t}{\partial x} + uA_y\frac{\partial k_t}{\partial y + wA_z\frac{\partial k_t}{\partial z}}\right) = -\varepsilon_t + P_t + G_t + diff_{k_t} \quad (12)$$

$$\frac{\partial \varepsilon_t}{\partial t} + \left(\frac{1}{\forall_f}\right)\left(uA_x\frac{\partial \varepsilon_t}{\partial x} + uA_y\frac{\partial \varepsilon_t}{\partial y + wA_z\frac{\partial \varepsilon_t}{\partial z}}\right) = \frac{-c_1.\varepsilon_t^2}{k_t +}\frac{c_2\varepsilon_t}{k_t(P_t + c_3.G_t)} + diff_\varepsilon \quad (13)$$

$$L_t = 0.164\frac{k_t^{1.5}}{\varepsilon_t}, \quad T_t = \frac{k_t}{\varepsilon_t} \quad (14)$$

In Eqs. 12-14, P_t, G_t, *diff* $_k$, and *diff* $_\varepsilon$ represent the kinetic energy and buoyancy production, as well as the diffusion terms, corresponding to k_t, andε_t,respectively. Among the advantages of the *k-ε* model are its relatively simple form, significant predictive power and high accuracy. According to Eq. 12, the energy and dissipation rate are proportional to the turbulence length (L_t) and time scale (T_t). The length and time scales are equivalent to the geometric scales and duration of the turbulence fluctuations within the flow field.

2.3.2. Scouring model

This model predicts erosion, sedimentation and sediment dispersion. The scouring model can be applied to any flow. The sedimentation unit

of the model assumes that the sediment particles are spherical and their velocity is low. The sedimentation rate is calculated as follows:

$$D_f = \frac{SCRDIA^2.RHOF}{18\mu} \quad (15)$$

In this equation, SCRDIA is the mean particle diameter; RHOF is fluid density; and μ is the dynamic viscosity of the fluid. Lifting rate is an experimental model based on bed load transfer models. The lift velocity is calculated from the following Eq:

$$Lift\ velocity = SCRALP\sqrt{\frac{\tau - \tau_c}{\bar{P}}} \quad (16)$$

In this equation, τ represents the amount of shear stress at the interface; ρ is macroscopic density of the fluid; SCRALP is an experimental parameter for adjusting the erosion intensity in each specific application. Based on experimental data, its default value for sand is 1. τ_c is the critical shear stress. When the shear stress exceeds this value, the forces that cause the particles to erode become larger than the forces that prevent the particles from rising, resulting in erosion. The critical shear stress is calculated using the critical Shields parameter, SCRCRT.

$$\tau_c = SCRCRT.SCRDIA.g.(SCRRHO - RHOF) \quad (17)$$

In this equation, SCRCRT is the critical Shields number, SCRRHO is the sediment particle density and g acceleration due to gravity. If the sediment volume fraction is greater than or equal to the critical solid fraction (SCRFCR), sediments are considered to have unit mass. In this case, the mass density will be equal to SCRFCR × SCRRHO.

Therefore, areas with a sediment concentration greater than or equal to SCRFCR × SCRRHO are considered a mass and no fluid flow occurs. In areas where the volume fraction of sediments is higher than SCRFCR however less than SCRFCR, the drag model is activated. When the volume fraction of sediments is less than SCRFCR, the drag model is not activated but the viscosity increases according to the following formula :

$$\mu = \mu_0\left(1 - \frac{solid\ fraction}{SCRFCR}\right)^{-1.55} \quad (18)$$

The entrainment coefficient (0.005) was applied to scale the scour rates and fit the experimental data. The settling velocity controls the deposition equation.

2.3.3. Model validation

To calibrate the mathematical model, data from ten experiments with varying blockage sizes and flow rates were used. The specifications of the calibration tests for are in Table 3. The computational time of the model was highly sensitive to cell size; however, reducing the cell size (0.7 cm external mesh and 0.35 cm internal mesh), did not significantly alter the modeling results. The model execution time for meshes with nested blocks (1 and 0.5 cm) increased from 10 to 75 hours. On the other hand, one of the limitations in the simulation of the erodible bed is the ratio of d_{50} to mesh size, which should have a maximum of 0.1. Other sediment characteristics, such as the Shields number, were extracted within the appropriate range, based to the results of three tests. The description of the selected parameters and the results is provided in Table 4. The error rate of the continuity equation is revealed in Fig. 2a. The limit of the error rate shows satisfactory results, with a value of $\pm 10^{-9}$. Based on the convergence criteria, the residual values of iterations should be less than 0.001 (Galan and Gonzalez, 2020). Fig. 2b shows the velocity and pressure residual values for the validated model.

Table 3. Characteristics of calibration tests.

Test	Q, l/s	B, %	Cell size, m	Roughness size, m
R1Q1B0	10.5	0	0.018	0
R1Q1B4	10.5	20	0.015	0.00085
R1Q1B8	10.5	40	0.015	0.00085
R1Q1B16	10.5	80	0.015	0.00085
R2Q2B0	16.5	0	0.015	0.00085
R1Q1B01	10.5	0	0.010	0.001
R1Q1B41	10.5	20	0.010	0.001
R1Q1B81	10.5	40	0.010	0.001
R1Q1B161	10.5	80	0.007	0.001
R2Q2B01	16.5	0	0.007	0.001

Table 4. Characteristics of simulated bed materials.

d_{50s}, cm	θ_{cs}	d_{50s}/δ_s	d_{smax}, cm
0.2	0.05	0.5	7.7
0.18	0.05	0.18	8.1
0.14	0.05	0.14	8.1
0.14	0.03	0.14	8.3
0.1	0.03	0.1	8.5

To increase the accuracy of the calibrated model, changes were made to the roughness height of the culvert barrel. First, the equivalent height of the bed roughness was set to 0.00085 m (glass roughness height), and then it was reduced to 0.001 m. The model guide introduces changes in wall roughness as an option to improve model performance in cases where it is not cost-effective to refine the grid structure, even if this value is not physically and realistically descriptive. In this table, d_{50s} is the size of homogeneous sediments, θ_{cs} is the critical Shields number, d_{50s}/δ_s is the ratio of sediment size to the size of the computational cell and, d_{smax} is the maximum depth of the simulated scour. The stability and strength of the mesh were controlled using the length-to-width ratio of the cell (maximum allowable value equal to 3) and the ratio of adjacent cells (the maximum allowable value is equal to 1.25) which were equal to 1.75 and 0.8, respectively. Both criteria were within the stable mesh range. Additionally, the degree of conformity of the blocks and the minimum amount of transfer error between the blocks, the criterion of the ratio of internal blocks were used, which was less than 2 and equal to 1.1 in the allowable range.

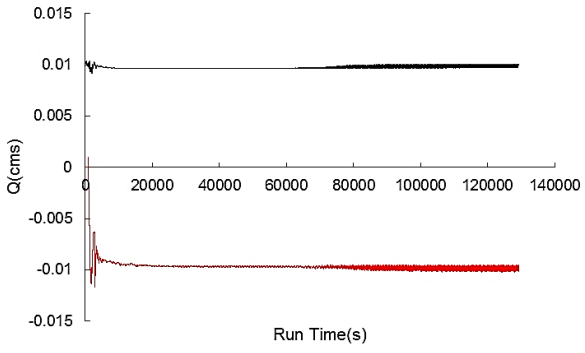

(a)

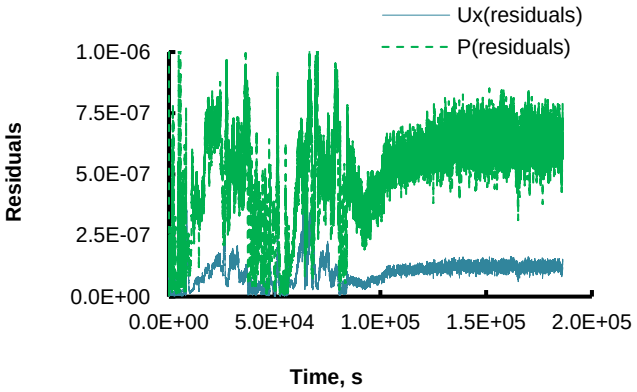

(b)

(c) (d)

Fig. 2. Calibrated model properties; (a) Inlet and outlet discharge consistency; (b) The velocity and pressure residual values; (c) Model geometry; (d) Validated mesh quality.

2.4. Boundary condition

The canal inlet was defined as the volume flow rate. The canal outlet was defined as specific pressure for any flow rate. The right side, the left side, and the bottom of the canal boundary were defined as walls. The top boundary defined as specified pressure with atmospheric pressure.

2.3.5. Modeling time determination

The model achieved hydraulic equilibrium at 80 seconds; However, equilibrium in the scouring hole was not established at this point. Figure 3 illustrates the process of stabilizing the maximum scouring depth. By 400 seconds, 95 % of the equilibrium depth was reached, and by 700 seconds, the maximum scour depth had nearly stabilized.

3. Results and discussion

Increasing the relative upstream energy of the culvert (ΔE/E) is the most important effect of reducing the inlet cross-section of the culvert. Figure 4 shows the variations of this parameter for all culvert models across different discharges. All sections for the design discharge (Q_d) show the lowest ΔE/E increases for the same obstruction. In the case of lower discharges, the ΔE/E values increase with increasing flow rate. Two-barrel models, in both types of cross-sectional shapes, show a greater increase than single-barrel models. This trend is not universal but is evident in lower discharges and obstructions of more than 40%. A more thorough examination of the results between the four culvert models, according to Fig. 5, shows a further increase in ΔE/E the C2 model. The higher upstream level of C2 for the same discharge compared to C1 is due to the larger inlet span of the C2 model than the other models under study.

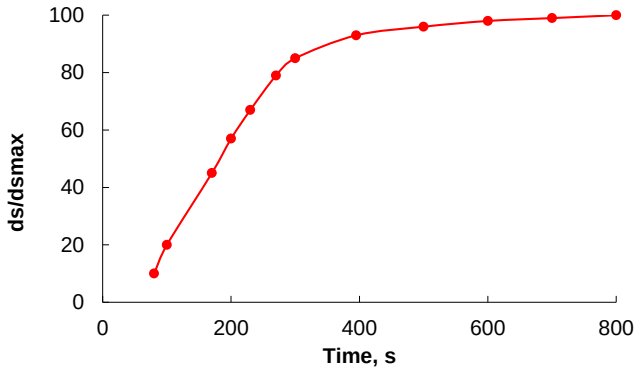

Fig. 3. Relative simulated scour depth (d_s/d_{smax}) versus time.

With an increase in relative upstream energy and stable downstream flow conditions, the outlet jet's erosive power also intensifies (Barthelmess and Rigby, 2011; Abida and Townsend,1991). Another factor that affects the strength of the outlet jet is the hydraulic jump formed in the culvert, which is influenced by various factors such as flow rate, downstream submergence, and cross-sectional shape. In contrast, the formation of hydraulic jumps would lead to a decrease in scouring risk downstream of the culvert (Ho and Muste and Ettema, 2013).

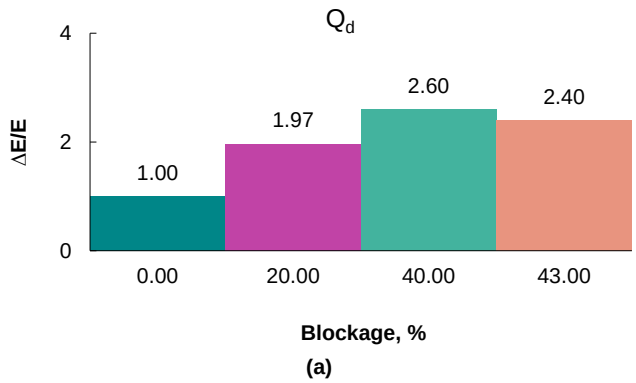

(a)

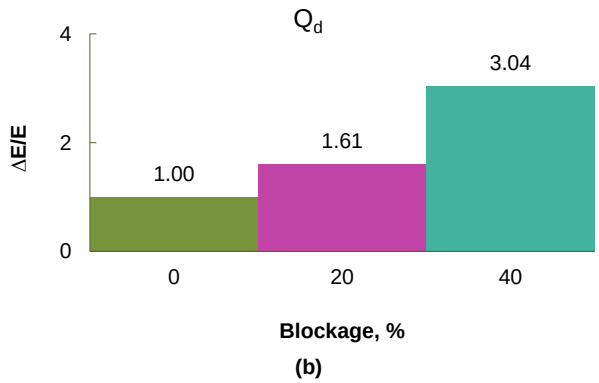

(b)

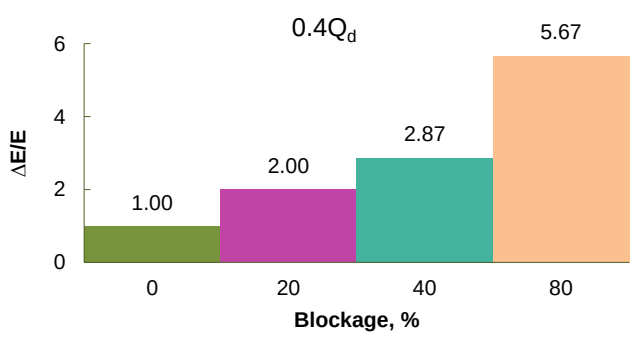

(c)

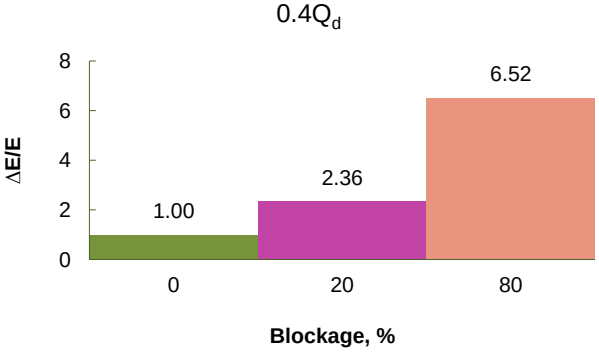

(d)

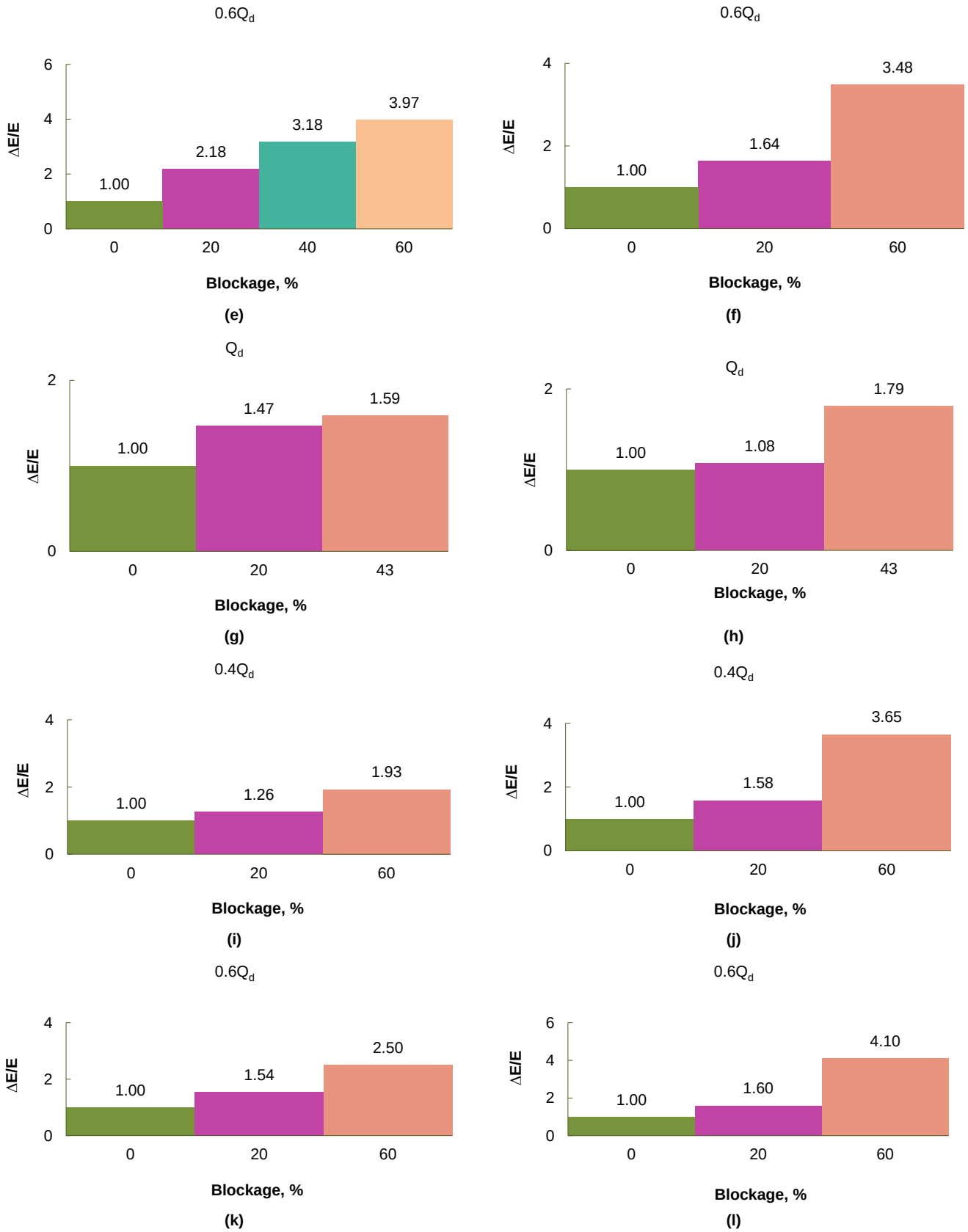

Fig. 4. Comparison of relative upstream energy of the culvert (ΔE/E) in different size of blockage for (a) Design discharge (Q_d) and one-barrel rectangular culvert(R1) ,(b) Design discharge (Q_d) and two-barrel rectangular culvert (R2), (c) 40% design discharge ($0.4Q_d$) and one-barrel rectangular culvert(R1), (d) 40 % design discharge ($0.4\ Q_d$) and two-barrel rectangular culvert (R2), (e) 60% design discharge ($0.6Q_d$) and one-barrel rectangular culvert (R1), (f) 60% Design discharge ($0.6\ Q_d$) and two-barrel rectangular culvert (R2), (g) Design discharge(Q_d) and one-barrel circular culvert (C1), (h) Design discharge (Q_d) and two-barrel circular culvert (C2), (i) 40 % design discharge (Q_d) and one-barrel circular culvert (C1), (j) 40% design discharge (Q_d) and two-barrel circular culvert (C2), (k) 60% design discharge (Q_d) and one-barrel circular culvert (C1), (l) 60% design discharge (Q_d) and two-barrel circular culvert (C2).

The interaction of these factors in the development of the scour hole leads to changes that are extremely complex and not easily predictable. The final changes in the downstream scour hole will be in reflect the results of this interaction. For this reason, it is not possible to suggest a general trend for changes in the scouring geometry downstream of the culvert due to obstruction without considering the hydraulic conditions of the culvert and downstream channel.

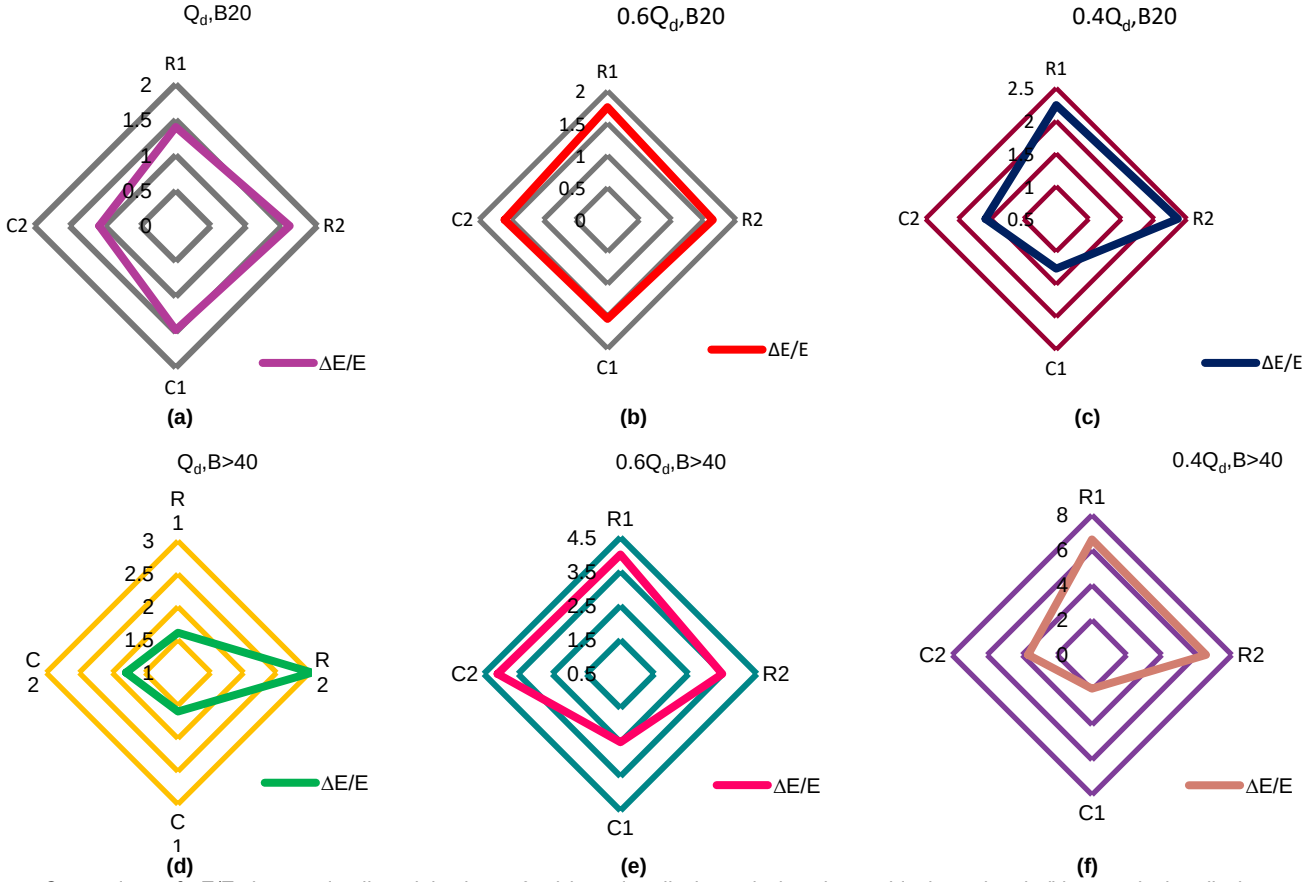

Fig. 5. Comparison of ΔE/E changes in all model culverts for (a) Design discharge(Q_d) and 20 % blockage (B20), (b) 60 % design discharge ($0.6Q_d$) and 20 % blockage (B20), (c) 40 % Design discharge ($0.4Q_d$) and 20% blockage (B20), (d) Design discharge(Q_d) and more than 40 % blockage (B>40), (e) 60 % Design discharge ($0.6Q_d$) and more than 40 % blockage (B>40), (f) 40 % Design discharge ($0.4Q_d$) and more than 40 % blockage (B>40).

Fig. 6 shows $\frac{\zeta^B_{smax}}{\zeta^0_{smax}}$ the exchange $\frac{\Delta E}{E}$ for all models. The data is classified according to downstream relative submergence($\frac{H_t}{D}$). It should be noted that the lowest relative submergence value corresponds to the lowest discharge while the highest value corresponds to the Q_d. Relative downstream depth values for all models were selected based on Abida and Townsend, 1991's analysis in the range that is practically the most common operating range ($0.2 \leq \frac{H_t}{D} \leq 0.8$) and outside this range, scour depth varies with tailwater depth in a completely different manner.

According to Fig. 5 and Fig. 6, for a culvert model, $\frac{\zeta^B_{smax}}{\zeta^0_{smax}}$ is directly related to $\frac{\Delta E}{E}$, but the trend of change is different for different discharge values. For R1 and R2, the trend is almost the same, although there are differences in values (Fig. 6a). For $0.4Q_d$ and B>40%, R2 and R1 have the highest $\frac{\Delta E}{E}$ and $\frac{\zeta^B_{smax}}{\zeta^0_{smax}}$ values (6.52 and 3.8 respectively). All sections almost have the same $\frac{\Delta E}{E}$ rate for 0.6 Q_d and all blockage values, but the C2 model culvert has the highest $\frac{\Delta E}{E}$ and $\frac{\zeta^B_{smax}}{\zeta^0_{smax}}$ values for 0.6 Q and more than 40% blockage (4.2 and 2.7 respectively).

In the case of Q_d, the C2 model shows the lowest $\frac{\Delta E}{E}$ per 20% blockage, and in the case of blockages greater than 40%, the R2 model shows the highest increase in $\frac{\Delta E}{E}$ values. The changes of $\frac{\zeta^B_{smax}}{\zeta^0_{smax}}$ values in this case are less for all models than those for other other flow rates tested. However, rectangular models show greater $\frac{\zeta^B_{smax}}{\zeta^0_{smax}}$ values than the circular models.

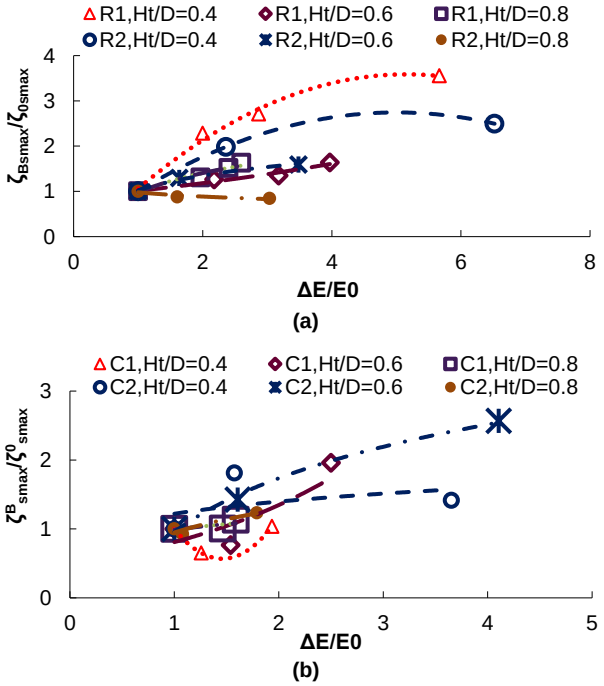

Fig. 6. $\frac{\zeta^B_{smax}}{\zeta^0_{smax}}$ changes against $\frac{\Delta E}{E}$ in (a) Rectangular model culverts and, (b) Circular model culverts.

Examination of changes in the maximum scour depth in the laboratory studies shows that, despite the constant downstream conditions, this parameter does not change significantly in the blocked culvert however; the effect of blockage on culvert efficiency is very significant (Taha *et al*., 2020). But this change in flow energy has caused a significant increase in the amount of $\frac{\zeta^B_{smax}}{\zeta^0_{smax}}$, as shown in Fig. 7. The changes in the relative maximum scour depth of the hole walls (d_{swall}/D) for all four studied models are shown in Fig. 7.

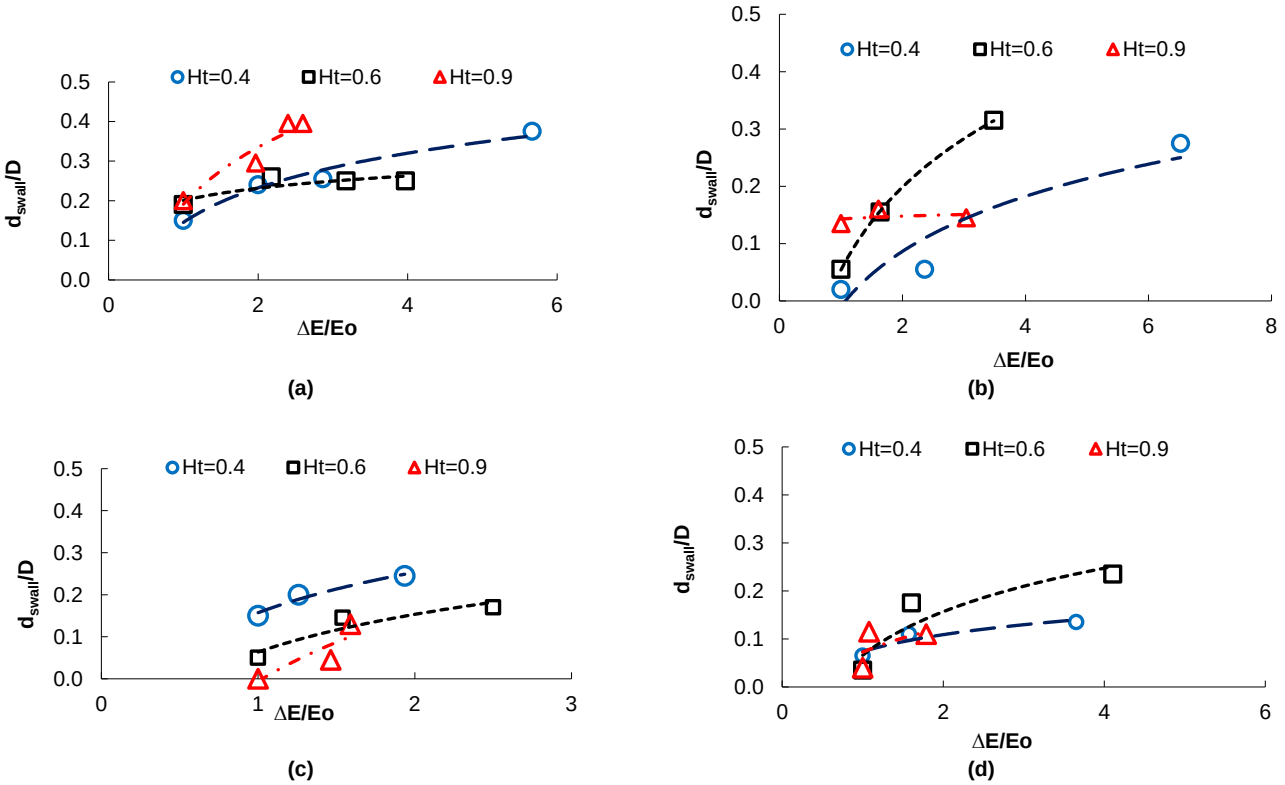

Fig. 7. Changes of d_{swall}/D against $\Delta E/E_0$ in (a) R1, (b) R2, (c) C1 and, (d) C2.

Increased scouring depth along the walls is evident for all models. Increased wall scouring depth for the R1 and R2 models being greater than C1 and C2 models. The $\frac{\Delta E}{E}$ increase in rectangular culverts due to the presence of obstruction is 1.5 to 3 times greater than that in circular culverts. The d_{swall}/D values for R1 and R2 culverts are 0.4 and 0.32, respectively, while the values for C1 and C2 culverts are 0.27 and 0.25, respectively.

The internal structure of the flow in the culvert, under the influence of the inlet blockage, was investigated using the simulated results of the calibrated numerical model. Fig. 8 shows a comparison of the values of the simulated scouring parameters against the measured values. The results indicate that the agreement between the numerical and experimental modeling is quite good. The effects of inlet obstruction on scouring geometry components and downstream turbulence have been evaluated experimentally and numerically in previous studies (Smith, 1957; Taha *et al*., 2020). However, the effect of changes in the turbulence of the downstream flow on the scour geometry process has not been reported thus far. Determining the impact of these changes is essential for identifying vulnerabilities and retrofitting operations. Fig. 9 shows a comparison of the simulated transverse profiles with the laboratory profiles for R1 and R2 culverts at the maximum scour depth. Examination of the profiles shows that the location of the maximum scour depth has shifted towards the walls. This is a common point between the laboratory and simulated profiles, despite the many differences that can be seen in them.

The reason for this movement is found in the process of changing the local velocity components. To avoid cluttering, in this section the results of design discharge and 40% and 60% blockage presents the results graphically Figure 10 shows velocity component distribution in blocked and non-blocked culverts. The maximum velocity in the direction of flow (v_x) is 1.2 times higher with the presence of the 40% blockage. In the non-blocked case, the maximum v_y component is $0.13v_x$ at $Y = 0.3w$ and the maximum v_z component is $0.1v_x$ at $Y = 0.3w$. With a 40% obstruction, these values for v_y and v_z are $0.23v_x$ at $Y = 0.1w$ and $0.16v_x$ at $Y = 0.1w$, respectively.

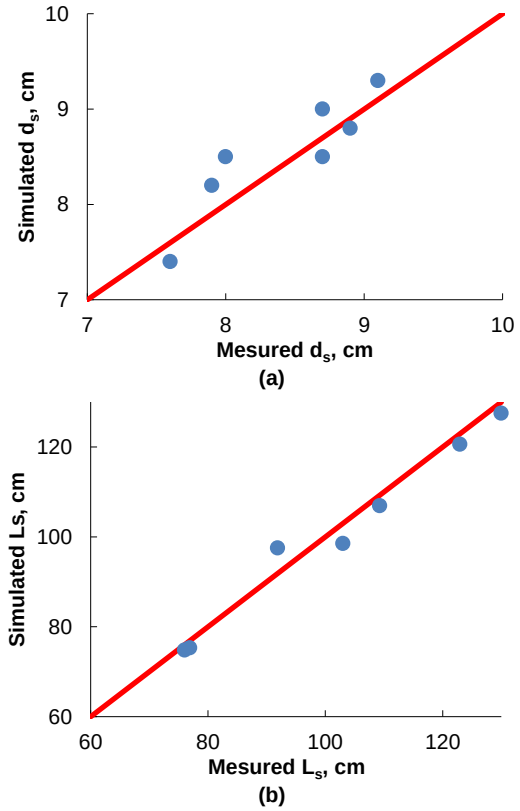

Fig. 8. Comparison of simulated values against measured values, (a) d_s, (b) L_s.

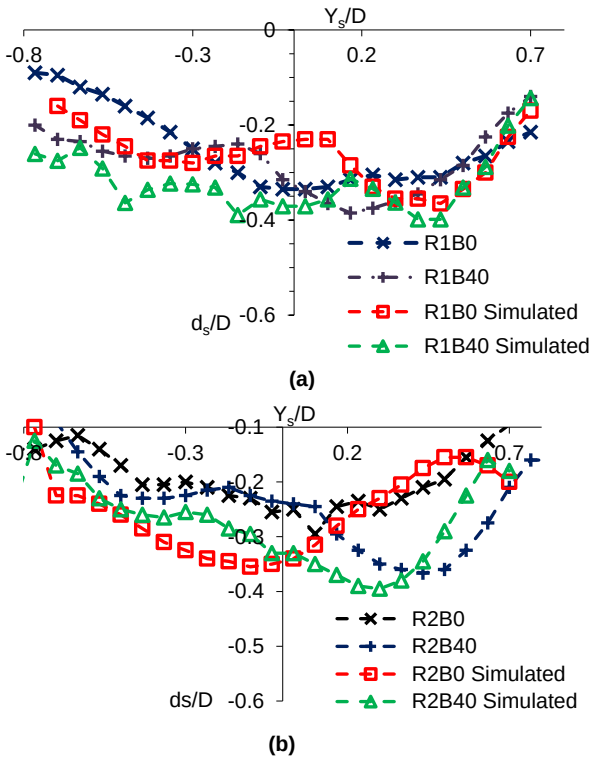

Fig. 9. Comparison of simulated and measured transverse scour profiles along ds, (a) R2, (b) R1.

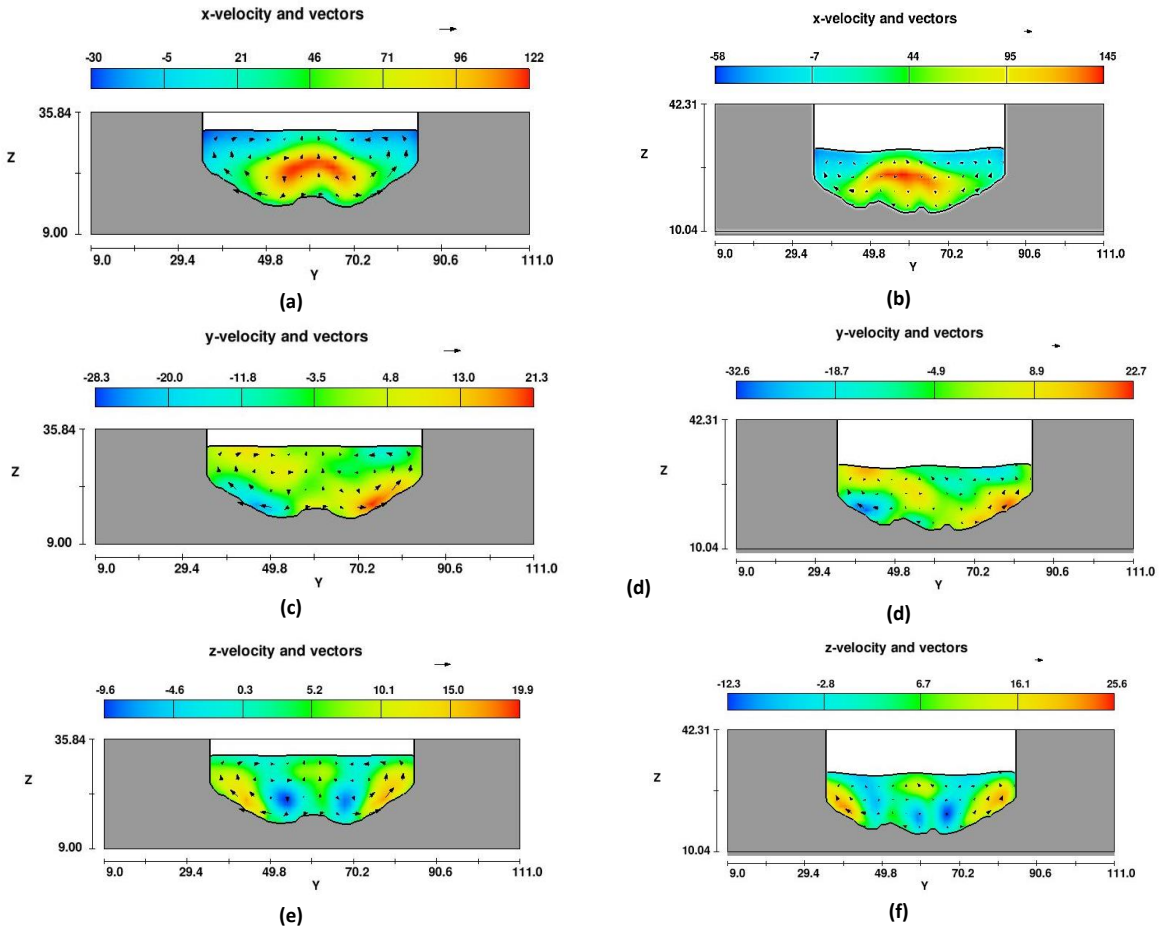

Fig. 10. Velocity components distribution, (a) R1B0v_x, (b) R1B40v_x, (c) R1B0v_y (d) R1B40v_y, (e) R1B0v_z, (f) R1B40v_z.

Differences in the magnitude and location of maximum velocity components are observed, accompanied by asymmetry due to the presence of an obstruction. This asymmetry in the velocity distribution leads to increased vortex formation and negative pressure within the hole (Day and Liriano and White, 2002). Fig. 13 presents the dimensionless velocity components across three sections: the culvert inlet, the culvert outlet, and the point of maximum scour depth. These velocity components were made dimensionless using the upstream approximation velocity. The velocity distribution varies across all, all three sections, both with and without obstruction. In the presence of obstruction, the maximum streamwise velocity (v_{xmax}) at the outlet of the culvert and the location of the maximum scour depth are 2.4 and 2

times greater than in the non-blocked condition, respectively (Fig. 11(b), 11(e), 11(c) and 11(f)). The location of the v_{xmax} in the blocked inlet is closer to the bed than in the non-blocked inlet. The increase in the streamwise mean velocity v_{xmax} and the negative values in the vertical components of the velocity ($v_y$andv_z) confirm the existence of strong secondary currents. Increased local turbulence at the outlet of the culvert is the main reason for the change in the geometry of scour hole.

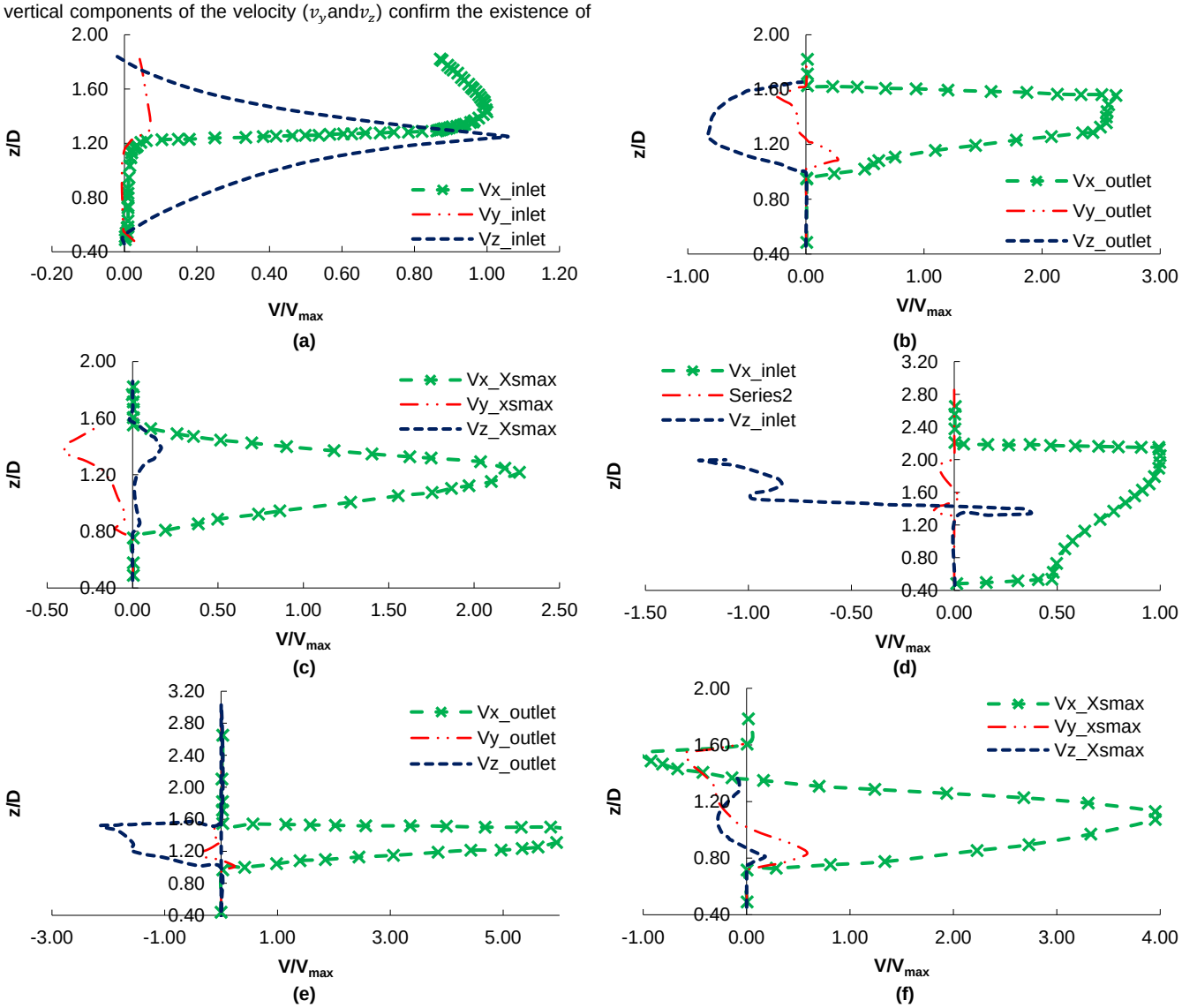

Fig. 11. Dimensionless velocity components distribution in, (a) R2B0 inlet, (b) R2B0 outlet, (c) R2B0 X_{smax}, (d) R2B60 inlet, (e) R2B60 outlet, (f) R2B60 X_{smax}.

According to previous data, even the slight amount of obstruction increases the energy difference and consequently, increasing the energy difference enhances the hydraulic jump (Pagliara and Carnacina, 2011). Enhanced hydraulic jump is the most effective factor for changes in the scour hole. In the initial moments of the blockage at the inlet of culvert, the $\frac{\Delta E}{E}$ is maximum and the jump is amplified. As time passes, the increased turbulence increases accelerate the rate of scouring. Eventually the flow will be reaching a balance. As the $\frac{\Delta E}{E}$,values decrease and the hydraulic jump weakens, the erosive power of the current also decreases. For this reason, for the same F_{rd}at the outlet, the maximum scour depth is much lower for an obstructed inlet compared to a non-obstructed flow. Thus, the equations that were previously presented for estimating scour depth have estimated the scour depth with a large error margin for the culverts with obstructions. Taha *et al*., 2020's studies also confirm these results. In order to evaluate an applied formula with acceptable accuracy, the previous relations provided for culverts without obstruction and with obstruction were used. Part of the laboratory data was used to present the formula, and another part was used for calibration. Finally, the calibrated numerical model was used to estimate the maximum scour depth for different values of obstruction and discharge. The predictor equations are evaluated as follows:

For Rectangular culvert: $\frac{d_s}{D} = \alpha F_{rd}^{0.83} (\frac{H_t}{D})^{-0.56} (\frac{R_h}{D})$ (18)

For Circular culvert: $\frac{d_s}{D} = \beta F_{rd}^{0.83} (\frac{H_t}{D})^{-0.56} (\frac{R_h}{D})$ (19)

The α and β coefficients will be defined based on $\frac{H_t}{D}$ and F_{rd} values. For condition of current study ($\frac{0.4<H_t}{D} < 0.9$ and $2.5 < F_{rd} < 8$) $\alpha = 0.41$ and $\beta = 0.46$.

Fig. 12a shows a comparison of the predicted data with the previously presented formulas. It can be clearly seen that the data obtained from previous relationships, such as (Bodhaine, 1968; Pagliara and Carnacina, 2011; Wang and Uys and Chanson, 2018; Zhang and Wu, 2019) using the laboratory data from the present study are very erroneous. In fact, estimating the maximum scour depth using these relationships is overestimated (Fig. 12a).

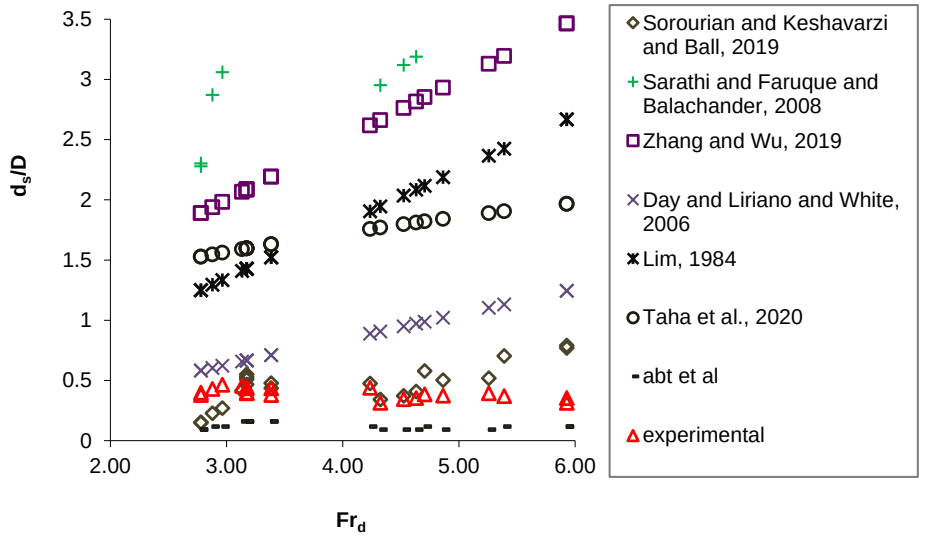
3.5
3
2.5
2
1.5
1
0.5
0
2.00
3.00
4.00
5.00
6.00
d_s/D
Fr_d
Sorourian and Keshavarzi and Ball, 2019
Sarathi and Faruque and Balachander, 2008
Zhang and Wu, 2019
Day and Liriano and White, 2006
Lim, 1984
Taha et al., 2020
abt et al
experimental

(a)

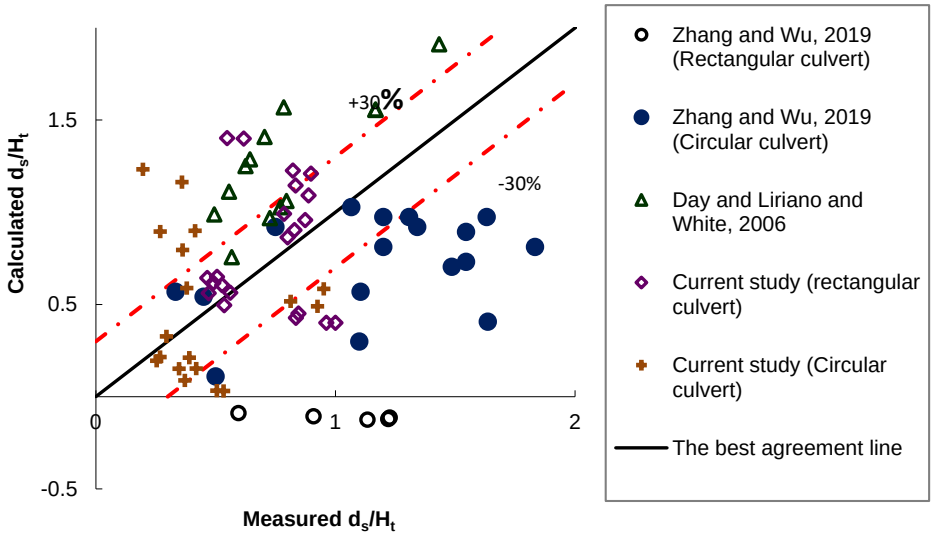
1.5
0.5
-0.5
0
1
2
+30%
-30%
Calculated d_s/H_t
Measured d_s/H_t
Zhang and Wu, 2019 (Rectangular culvert)
Zhang and Wu, 2019 (Circular culvert)
Day and Liriano and White, 2006
Current study (rectangular culvert)
Current study (Circular culvert)
The best agreement line

(b)

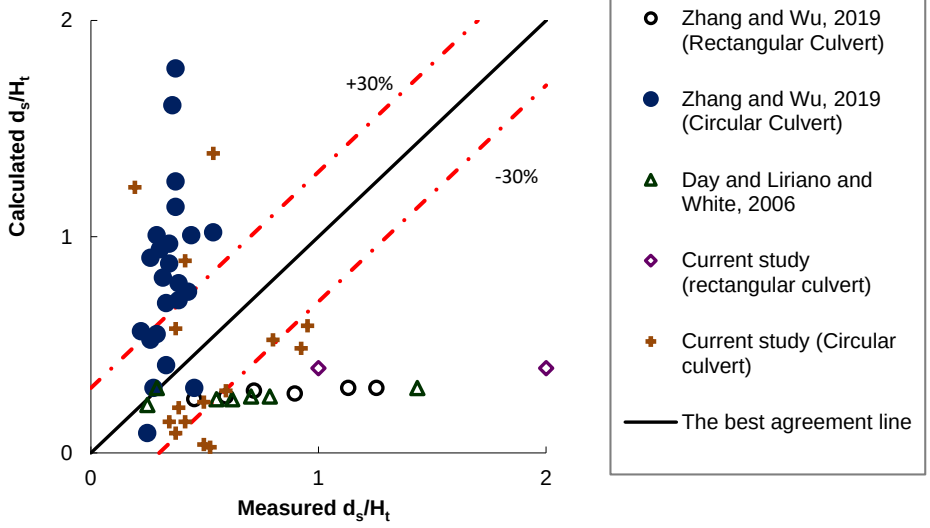
2
1
0
0
1
2
+30%
-30%
Calculated d_s/H_t
Measured d_s/H_t
Zhang and Wu, 2019 (Rectangular Culvert)
Zhang and Wu, 2019 (Circular Culvert)
Day and Liriano and White, 2006
Current study (rectangular culvert)
Current study (Circular culvert)
The best agreement line

(c)

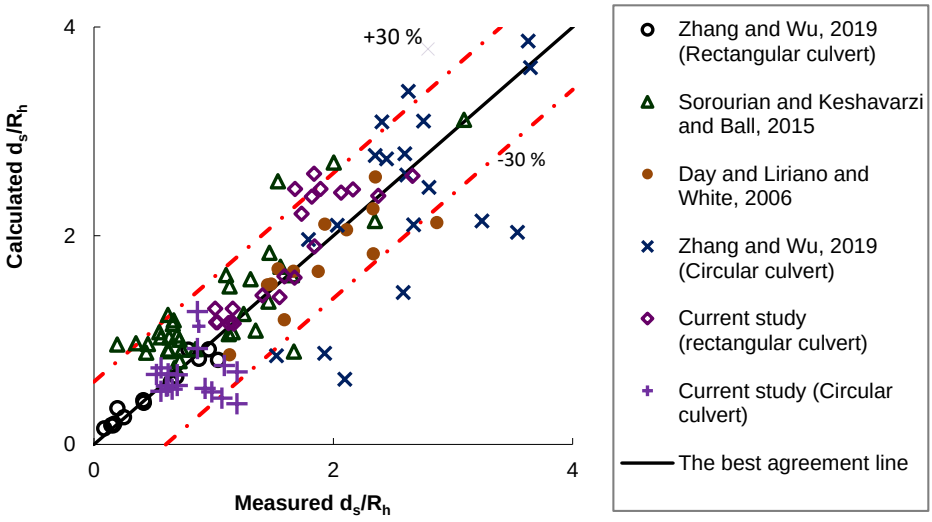

(d)

Fig. 12. Comparison of maximum depth predictor equations, (a) Performance of previously presented formulas based on culvert without obstruction in estimating laboratory data, (b) Performance of Sorourian and Keshavarzi and Ball, 2015's formula, (c) Performance of Taha *et al.,* 2020's formula, and (d) Performance of current formula.

Table 5. Prior predictor equations.

Equation	Remarks		Reference
$\frac{d_{sm}}{D} = 1.45F_{rd}$ * $\frac{d_{sm}}{D} = 4.5F_{rd}$ **	Derived from the equation proposed by Breusers and Raudkivi(1991) for circular jets	• $F_{rd} = 2.5 - 24.6$ • $d_{50} = 1.65\ mm$ • $1 \le F_{rd} \le 10$ * • $10 < F_{rd}$ **	Lim,1995
$\frac{d_{sm}}{D} = \alpha F_{rd} + \beta$ $\alpha = 0.88(H_t/D)^{-0.37}$ $\beta = 0.21\ln(H_t/D) - 0.26$	• Circular jets	• $0.5 \le H_t/D \le 2$ • $F_{rd} = 3.18 - 8.5$	Day and Liriano and White, 2002
$\frac{d_{sm}}{D} = 2.25\ln(F_{rd}) - 2.44$ *** $\frac{d_{sm}}{D} = a\ln(F_{rd} - b)$ **** $a = -0.66\left(\frac{H_t}{D}\right) + 2.34$, $b = 1.31\left(\frac{H_t}{D}\right)$-1.73	• Circular jets • F_{rd}=3.9-10 • $d_{50} = 0.71 - 2.46$	• $\frac{H_t}{D} = 4$ *** • $0.5 \le \frac{H_t}{D} \le 3$ ****	Sarathi *et al*., 2008
$\frac{d_{sm}}{h_d} = 0.27F_{rd} + 0.29B - 0.35$	• Box culvert • F_{rd}=1.5-13.3	• $d_{50} = 0.85{,}2\ mm$	Sorourian and Keshavarzi and Ball, 2015
$\frac{d_s}{R_h} = SH \times 0.66(F_{rd})^{0.82}(\frac{h_t}{R_h})^{-0.12}$	SH=1.54 for rectangular culverts SH=1.16 for circular culverts	• F_{rd}=0.21-0.72 • $d_{50} = 0.85{,}2\ mm$ (rectangular culverts) • F_{rd}=2.4-12.1 • $d_{50} = 0.03 - 0.2\ mm$(circular culverts)	Zhang and Wu, 2019
$\frac{d_{se}}{R_h} = 1.03F_{rd84}[e^{-1.9(K_s-1.2)^2} + 1]$	F_{rd84}= Densimetric Froude number based on D_{84} K_s=d_{50}/R_h	• F_{rd84}=22.27-52.86 • $d_{50} = 1.11, 3.06\ mm$	Zhao *et al*., 2019
$\frac{d_{sm}}{h_d} = 0.067F_{rd} + 0.16B_d + 0.11B_u - 0.245S + 0.224$	B_d =Blockage ratio in lower part of culvert B_u =Blockage ratio in upper part of culvert	• F_{rd}=4.7-8.3 • $d_{50} = 4\ mm$ • B=10, 20 and 30%	Taha *et al*., 2020

These equations are based on culvert studies without obstruction. The data obtained from equations that considered the effect of obstruction in studies (Sorourian and Keshavarzi and Ball, 2015; Taha et al., 2020) show better agreement with current experimental data (Fig. 12(b) and Fig.12(c)). However, they exhibit more errors in the data obtained from experiments performed on unblocked culverts. In particular, the equation of Sorourian and Keshavarzi and Ball, 2015 which is presented algebraically and has a constant value of -0.35, leads to negative results that are not physically defined (Fig.12(b)). Additionally, Taha *et al*., 2020's formula has an algebraic form with a constant value of +0.224 and shows highly overestimated values for Zhang and Wu, 2019's and Day and Liriano and White, 2001's data. All the compared equations presented in Table (5). All previous equations presented in the field of culvert scouring are exponential, linear, logarithmic or power functions of effective factors such as F_{rd} and $\frac{H_t}{D}$. It seems that the effect of obstruction on changes in scour geometry is more complex than merely adding the amount of obstruction algebraically to the scour formula.

As discussed in the previous sections, blockage affects the flow structure. The formula presented in this paper is based on laboratory and numerical data, focusing on the most effective factors (F_{rd}, R_h/D). When F_{rd} increases for a given flow, the flow depth eventually

decreases. The rate of depth reduction is a function of the cross-sectional shape. The hydraulic radius is the best geometric component of the flow that can demonstrate these properties. For this reason, the proposed equation is better suited for scour data in culverts with and without obstruction (Fig.12 d). It is evident that over 80 % of the datasets fall within ±30% error lines, while this is about 40 % for previous equations.

4. Conclusions

In this study, a series of laboratory experiments were conducted to investigate the effect of culvert inlet obstruction on culvert hydraulics and downstream scour hole geometry. Circular and rectangular culverts with different barrel numbers were used for this purpose. All tests were conducted under unsubmerged outlet conditions ($H_t/D < 1$). To complete the investigation, a set of numerical modeling was performed using the VOF method and the RANS turbulence model. The results showed that for a given value of inlet obstruction, the design discharge (Q_d) has the lowest $\Delta E/E$ value compared to $0.4Q_d$ and $0.6Q_d$. Furthermore, in the case of Q_d blockages, the C2 model shows the lowest $\Delta E/E$ value at 20% blockage. In contrast, for blockages greater than 40%, the R2 model shows the highest increase in $\Delta E/E$ values. Additionally, the changes in the relative volume of the scour hole ($\frac{\zeta_{smax}^{B}}{\zeta_{smax}^{0}}$) values for Q_d case for all models are less than those at $0.4Q_d$ and $0.6Q_d$. The results also indicated that d_{swall}/D grows in the blocked inlet condition more than d_{smax}/D. The d_{swall}/D values of rectangular model culverts were 1.3 to 1.5 times greater than those of circular model culverts. Although the circular model culvert yielded a more conservative volume of scour than the rectangular culvert in B > 0 values, the values of $\Delta E/E_o$ in the C1 and C2 model culverts had a lower rate of increase; consequently, d_{swall}/D exhibited less growth under the same flow and blockage conditions compared to the R1 and R2 model culverts. This answers the first question, showing that culvert shape and the number of barrels affect scour hole characteristics. In response to the second fundamental question, the results showed that blockage has a significant effect on scour hole characteristics, but not in a specific direction. In fact, culvert shape and flow conditions affect scouring progress. Based on the analysis of the data, new equations were found to be more reliable than the existing formulas. These formulae were presented with consideration of debris accumulation's effect on culvert outlet jet characteristics, such as, F_{rd} and R_h values. The newly presented equations were compared to previous equations by applying collected datasets and showed superior performance, indicating that over 80% of the predicted values fall within ±30% error margins.

Author's Contribution

The corresponding author guide scientifically and supported financial needs of the research and contributed in writing and revising the paper. The second author, handled all tasks including data collecting, writing, analyzing and numerical simulation.

Conflict of Interest

The authors declare that they have no known competing financial interests or personal relationships that could have appeared to influence the work reported in this paper.

Acknowledgement

The authors express their gratitude to Bu-Ali Sina University, Hamedan, Iran, for supporting in this research.

Data Availability Statement

The data that support the findings of this study are available from the corresponding author upon reasonable request.

Nomenclature

A	Cross- sectional area
B	Blockage of culvert iterance
C	Conveyance coefficient
C1	One-barrel circular culvert
C2	Two-barrel circular culvert
d_c	Critical depth at the culvert inlet
d_s	Scour depth
d_{swall}	Scour depth near downstream wall
d_{50}	Mean diameter of sediments
diff $_k$	Diffusion term
diff $_e$	Diffusion term
$E_{downstrea m,B}$	The total hydraulic energy at the downstream in the presence of debris accumulation
E_0	The difference between the upstream and downstream energy values
fr_d	Froud number
g	Gravity acceralation
G_t	Buoyancy production
H_f	Energy loss
H_t	Tailwater depth
K_{ed}	Diffusivity
L_s	Length of scour hole
L_t	The turbulence length
Q	Discharge
Q_d	Design discharge
P_t	Kinetic energy
RHOF	Fluid density
R1	One-barrel rectangular culvert
R2	Two-barrel rectangular culvert
Sc	Schmidt's number
SCRDIA	The mean particle diameter
T_t	Time scale
V	Velocity
Vf	Volume fraction
Z	Culvert bottom elevation
α	Coefficient defines based on $\frac{H_t}{D}$ and F_{rd} values
β	Coefficient defines based on $\frac{H_t}{D}$ and F_{rd} values
υ_t	Eddy viscosity
μ	Dynamic viscosity of the fluid
τ_c	Critical shear stress
ρ	Macroscopic density of the fluid
ρ_s	Density of the sediment
ω_s	Weigh of sediment
χ_s	Width of scour hole
ζ_s	Length of scour hole

References

Abida, H. and Townsend, R. D. (1991) 'Local scour downstream of box-culvert outlets', *Journal of Irrigation and Drainage Engineering*, 117(3), pp. 425-440. doi: https://doi.org/10.1061/(ASCE)0733-9437(1991)117:3(425)

Allen, D. *et al*., (2015) 'Provision, transport and deposition of debris in urban waterways', *International Journal of Sediment Research*, 30(2), pp.142-149. doi: https://doi.org/10.1016/j.ijsrc.2015.03.006

Armitage, N. P. and Rooseboom, A. (1999) 'The removal of litter from storm water conduits in the developing world', *Water Science and Technology*, 39(9), pp. 277-284. doi: https://doi.org/10.1016/S0273-1223(99)00242-5

ARR (2009) *P11/S1/007: Blockage of hydraulic structures*. Available at: https://arr.ga.gov.au/__data/assets/pdf_file/0010/40510/ARR_Project_11_Stage1_report_Final.pdf (Accessed date: 8 December 2024).

CIRIA (2010) *SC070038/S1*: *Culvert design and operation guide*. Available at: https://assets.publishing.service.gov.uk/media/6032d842d3bf7f7223f00039/Culvert_Design_Guide_Summary.pdf (Accessed date: 8 December 2024).

Barthelmess, A. J. and Rigby, E. H. (2011) 'Estimating culvert and bridge blockages-a simplified procedure', *Proceeding 34th World Congress International Association for Hydro-Environment Research and Engineering: 33rd Hydraulic and Water Research Symposium and 10th Conference on Hydraulic in Water Engineering*. 2011, Barton, ACT: Engineers Australia. Available at: https://search.informit.org/doi/abs/10.3316/informit.263819535468740 (Accessed date: 8 December 2024).

Bodhaine, G. L. (1968) *Measurement of peak discharge at culverts by indirect methods.* 1st edn. US Government Printing Office, Washington, DC.

Day, R. A., Liriano, S. L. and White, W. R. (2001) 'Effect of tailwater depth and model scale on scour at culvert outlets', *Proceedings of the Institution of Civil Engineers-Water and Maritime Engineering,* 148, (3), pp. 189-198. doi: https://doi.org/10.1680/wame.2001.148.3.189

Galan, A. and Gonzalez, J. (2020) 'Effects of shape, inlet blockage and wing walls on local scour at the outlet of non-submerged culverts: undermining of the embankment', *Environmental Earth Science*., 79(1), pp. 25-37. doi: https://doi.org/10.1007/s12665-019-8749-3

Ho, H. C., Muste, M. and Ettema, R. (2013) 'Sediment self-cleaning multi-box culverts', *Journal of Hydraulic Research,* 51(1), pp. 92-101. doi: https://doi.org/10.1080/00221686.2012.757565

Hotchkiss, R. H., Larson, E. A. and Admiraal, D. M. (2005) 'Energy dissipation in culverts by forced hydraulic jump within a barrel', *Journal of transportation Research Board*, 1904(1), pp. 124-132. doi: https://doi.org/10.1177/0361198105190400113

Liriano, S. L., Day, R. A. and White, W. R. (2002) 'Scour at culvert outlets as influenced by the turbulent flow structure' *Journal of Hydraulic Research*, 40(3), pp. 367-376. doi: https://doi.org/10.1080/00221680209499951

Melville, B. W. and Lim, S. Y. (2013) 'Scour caused by 2D horizontal jets', Journal of Hydraulic Engineering, 140(2), pp. 149-155. doi: https://doi.org/10.1061/(ASCE)HY.1943-7900.0000807

Pagliara, S. and Carnacina, I. (2011) 'Influence of large woody debris on sediment scour at bridge piers', International Journal of Sediment Research, 26(2), pp. 121-136. doi: https://doi.org/10.1016/S1001-6279(11)60081-4

Sarathi, P., Faruque, M. A. A. and Balachandar, R. (2008) 'Influence of tailwater depth, sediment size and densimetric Froude number on scour by submerged square wall jets', *Journal of Hydraulic Research*, 46(2), pp. 158-175. doi: https://doi.org/10.1080/00221686.2008.9521853

Smith, G. L., (1957) Scour and energy dissipation below culvert outlets. 1st edn. Colorado Agricultural and Mechanical College, Department of Civil Engineering, Colorado.

Sorourian, S., Keshavarzi, A. and Ball, J. E. (2015) 'Scour at partially blocked box-culverts under steady flow', *Proceedings of the Institution of Civil Engineers-Water Management*, 169 (6), pp. 247-259. doi: https://doi.org/10.1680/jwama.15.00019

Streftaris, G. *et al*. (2012) Modeling probability of blockage at culvert trash screens using Bayesian approach', *Journal of Hydraulic Engineering*, 139 (7), pp. 716-726. doi: https://doi.org/10.1061/(ASCE)HY.1943-7900.0000723

Taha N. *et al.* (2020) 'Numerical investigation of scour characteristics downstream of blocked culverts', *Alexandria Engineering Journal*, 59 (5), pp. 3503-3513. doi: https://doi.org/10.1016/j.aej.2020.05.032

Wallerstein, N. and Arthur, S. (2012) 'Improved methods for predicting trash delivery to culverts protected by trash screens', *Journal of Flood Risk Management*, 5(1), pp. 23-36. doi: https://doi.org/10.1111/j.1753-318X.2011.01122.x

Wang, H., Uys, W. and Chanson, H. (2018) 'Alternative mitigation measures for fish passage in standard box culverts: physical modelling', *Journal of Hydro-Environment Research*, 19, pp. 214-223. doi: https://doi.org/10.1016/j.jher.2017.03.001

Zhang, R. and Wu, P. (2019) 'The investigation of shape factors in determining scour depth at culvert outlets. *ISH Journal of Hydraulic Engineering*, pp. 1-7. doi: https://doi.org/10.1080/09715010.2019.1611492

Zhao, P., Yu, G. and Zhang, M. (2019) 'Local scour on noncohesive beds by a submerged horizontal circular wall jet', *Journal of Hydraulic Engineering*, 145(9), pp. 190-196. doi: https://doi.org/10.1061/(ASCE)HY.1943-7900.0001623